Multi-Objective Optimization Design of Permanent Magnet Eddy Current Coupler Based on SCG-BP Neural Network Modeling and the ONDX-NSGA-II Algorithm

Dazhi Wang [1,*], Bowen Niu [1], Pengyi Pan [1] and Guofeng Sun [2]

[1] College of Information Science and Engineering, Northeastern University, No. 3-11 Wenhua Road, Shenyang 110819, China; 2100806@stu.neu.edu.cn (B.N.); 2100808@stu.neu.edu.cn (P.P.)

[2] State Grid Shandong Electric Power Company Yantai Power Supply Company, No. 158 Jiefang Road, Yantai 264000, China; sgfvsjy@163.com

[*] Correspondence: wangdazhi@ise.neu.edu.cn; Tel.: +86-133-2245-2013

Abstract: There is a complex coupling relationship between the structural parameters and various performance indicators of a permanent magnet eddy current coupler. In order to obtain the optimal combination of structural parameters that can improve the overall performance of the coupler, it is necessary to reasonably balance the contradiction and competition among performance indicators of the permanent magnet eddy current coupler. A multi-objective optimization method for permanent magnet eddy current couplers based on scaled conjugate gradient back propagation neural network modeling, improved opposition-based learning, and normal distribution crossover operator non-dominated sorting genetic algorithm-II is proposed. The optimization results are compared with those of the traditional non-dominated sorting genetic algorithm-II and the Pareto envelope-based selection algorithm-II, and it is verified that the proposed multi-objective optimization algorithm is accurate, reliable, and has better convergence and versatility. Compared with the original model, the output torque of the optimized coupler increased by 8.54%, and the eddy current loss and cost decreased by 3.71% and 8.74%, respectively. Finally, the correctness of the theoretical analysis was verified through 3D finite element simulation and an experimental simulation platform.

Keywords: permanent magnet eddy current coupler; multi-objective optimization; scaled conjugate gradient back propagation neural network; non-dominated sorting genetic algorithm-II; opposition-based learning mechanism; finite element analysis

1. Introduction

Permanent magnet eddy current coupler (PMECC) is a new type of flexible, energy-saving driving component that connects motors and loads. It can achieve the transmission of output torque by adjusting the force between magnetic fields and has the advantages of no mechanical wear, soft start of the motor, and overload protection [1]. Compared to traditional mechanical transmission devices, PMECC not only reduces energy loss and maintenance costs but also extends equipment life and has the characteristics of silent operation. Compared to magnetic gears, the design of PMECC is relatively simple and does not require precise magnetic field control, making it more cost-effective in manufacturing and maintenance. In the field of wind turbines, PMECC connects wind turbine blades and generators and adjusts the rotational speed of wind turbine blades through precise torque control to adapt to different wind speed conditions, thereby improving the efficiency of wind power generation. In the field of water pumps, PMECC connects an electric drive and a water pump, achieving precise flow regulation of the water pump system by controlling torque output, improving equipment efficiency and operational accuracy, and reducing energy waste. In these application fields, permanent magnet eddy current couplings have improved the performance and operability of equipment through their

precise control characteristics and have had a positive impact in the fields of energy conservation and mechanical transmission. Therefore, it has broad application prospects in related transmission equipment such as fans and water pumps in the agricultural machinery industry [2–4]. The specific mechanical structure of PMECC is shown in Figure 1.
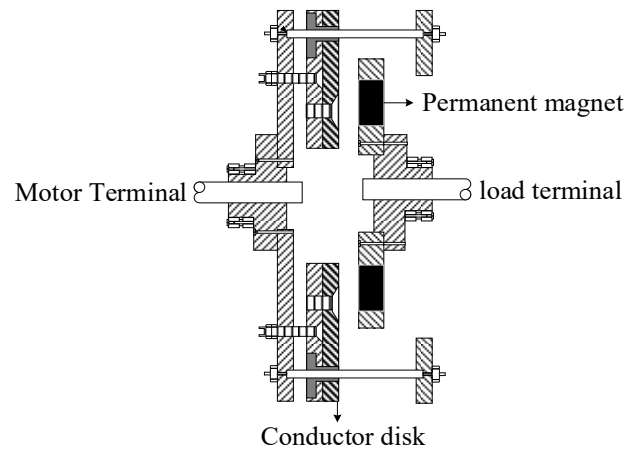
Figure 1. Structure of PMECC.

In recent years, research on PMECC has mainly focused on characteristic analysis and structural improvement design [5,6]. However, research on structural parameter optimization of PMECC is not yet sufficient. The research on optimizing the structural parameters of PMECC can help to balance as well as improve multiple performance indicators of PMECC, improve energy utilization efficiency, and reduce cost expenditure in order to achieve a more efficient, economical, and environmentally friendly design. Therefore, how to establish a mathematical model before optimization and how to carry out reasonable multi-objective optimization to effectively improve the overall performance of a coupler are currently hot research issues.

In terms of modeling PMECC, it is mainly divided into two categories: numerical modeling and analytical modeling. Numerical modeling methods can accurately calculate various physical fields and performance parameters. However, obtaining more accurate results requires a large amount of computation, lengthy computation time, and high equipment requirements [7,8]. Therefore, this method is not suitable for use in the early stages of coupler design and optimization [9,10].

The analytical modeling method simplifies and assumes the geometric shape or material properties of the coupler during the calculation process, which will result in the mathematical model being unable to accurately reflect the impact of all design parameters on the electromagnetic performance of the equipment [11,12]. The accuracy and generality of the method are poor.

In terms of optimization, reference [13] utilized the proposed hybrid particle swarm optimization simplex method algorithm to optimize the design of PM couplings, subject to several key design constraints. The hybrid algorithm has the prominent feature of combining global and local search capabilities; however, its analytical model is a two-dimensional analytical model solved using the separation of variables method with low accuracy. Reference [14] used artificial neural networks to obtain the mapping relationship between PMECC output torque and structural parameters and then optimized the structural parameters using the particle swarm optimization method to improve the output torque. However, due to the coupling relationship between multiple performance indicators of PMECC, optimizing only the output torque may lead to a decrease in the performance of other indicators; therefore, a compromise needs to be made between each performance indicator. Single-objective performance optimization cannot consider the advantages and disadvantages of other performances while optimizing one objective, and performance optimization is not comprehensive. Therefore, its applicability in PMECC optimization

design is limited. Reference [15] proposed a multi-objective particle swarm optimization algorithm for modeling and analyzing PMECC devices, which improved the radial magnetic flux density and transmission torque of the device and reduced eddy current losses. However, the weight, cost, and other factors of the PMECC were not considered in the research, and the optimization research was not comprehensive enough.

Reference [16] comprehensively considered the cost, output torque, and eddy current losses of permanent magnet drives and used an improved cuckoo search algorithm to optimize the solution. However, the performance indicators of PMECC in this paper were all obtained through analytical methods, and the calculation process was complex and inaccurate. Moreover, the multi-objective optimization algorithm mentioned above may also have a slow convergence speed and be prone to falling into local optima during the optimization process. Reference [17] aimed to optimize the electromagnetic torque and cost of PMECC and conducted multi-objective optimization based on an improved genetic algorithm. However, the eddy current loss of PMECC was not considered in this study, making it impossible to comprehensively improve the performance of PMECC. Moreover, a large amount of experimental sample data was required for modeling, greatly increasing the workload of the optimization process.

Based on the above analysis, this paper proposes a scheme that combines the scaled conjugate gradient back propagation (SCG-BP) neural network modeling and fast non-dominated multi-objective optimization algorithm with an elite reservation strategy based on improved opposition-based learning and normal distribution crossover operator non-dominated sorting genetic algorithm-II (ONDX-NSGA-II algorithm), with the output torque, eddy current loss, and cost of PMECC as the multi-objective optimization performance indicators. Firstly, the SCG-BP neural network is used to establish the models of the output torque and eddy current loss. Additionally, the cost model of PMECC is introduced as the third objective function. Secondly, the NSGA-II algorithm with an improved opposition-based learning mechanism and normal distribution crossover operator (NDX) is used as the optimization method to optimize the structural parameters of PMECC. This method has advantages such as fast convergence speed, a stable optimization process, and resistance to trapping in local optima. In addition, this method is compared with some algorithms in other literature to demonstrate its superiority. Finally, the applicability and effectiveness of the model established in this paper and the optimization algorithm used are verified through finite element simulation.

2. BP Neural Network Based on Scaled Conjugate Gradient Algorithm

This paper first established an SCG-BP neural network to achieve the mapping from PMECC parameters to its performance, thus obtaining the objective function to be established [18]. The schematic diagram of the SCG-BP neural network model is shown in Figure 2.
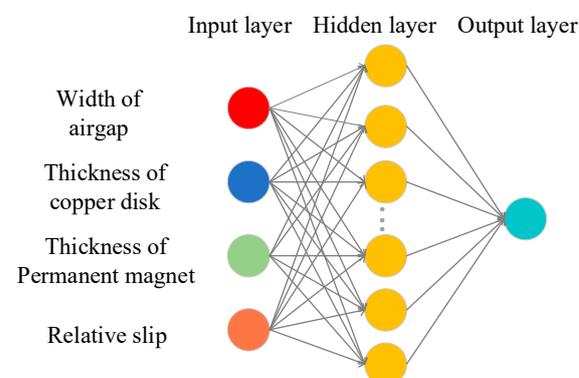
Figure 2. Structure of SCG-BP neural network model.

The four structural parameters of PMECC, including air gap width, thickness of the copper disk, thickness of permanent magnet, and relative slip, were selected as decision variables to optimize its performance. Within the constraint range, these parameters were changed by the control variables. The corresponding output torque and eddy current loss were calculated by the finite element model, and a total of 449 sets of structural parameters were obtained. Then, we randomly selected 315 cases as network learning training data, 67 cases as test data to evaluate the learning effectiveness of the neural network, and the remaining 67 cases as the validation set of the neural network.

2.1. Design of BP Neural Network Structure Based on Scaled Conjugate Gradient Algorithm

(1) Determine the total number of layers in the network. This design uses a three-layer network, which is the input layer, the hidden layer, and the output layer.
(2) Determine the number of nodes in the input layer. The number of input layer nodes depends on the number of input vectors; therefore, the neural network structure in this paper has four input nodes.
(3) Determine the number of hidden layer nodes. The number of hidden layer neurons in a BP network determines the complexity of the network [19,20]. The range of the number of hidden layer neurons is determined by Equation (1).

$$M = \sqrt{(m + n)} + a \tag{1}$$

In the equation, M is the number of neurons in the hidden layer, m and n are the number of neurons in the input and output layers, respectively, and a is a constant between [0, 10].

The specific number of hidden layer neurons is determined by the "step test procedure". In this paper, the range of the optimal number of hidden layer neurons is first calculated as [4,13] based on Equation (1) and then debugged one by one within this range.

During the training process, the mean square error (MSE) and regression value (R) are used to quantitatively analyze the accuracy corresponding to the number of neurons in each hidden layer.

The experiment started with 4 neurons and increased to 13, adding one neuron at a time. Each experiment is trained 100 times using 449 sets of samples, and the average values of MSE and R of all training results are taken as the final reference values. The experimental results are shown in Figure 3.

(**a**) Output torque
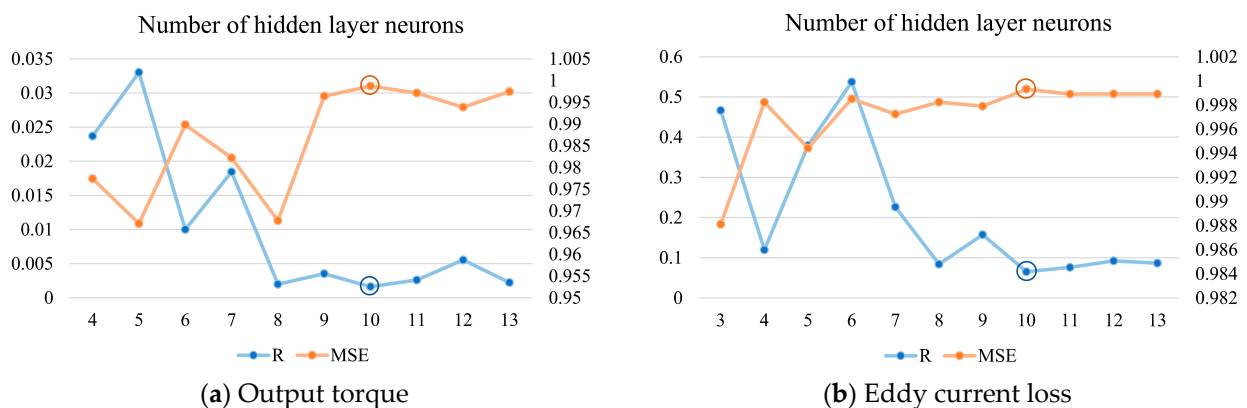
(**b**) Eddy current loss

Figure 3. Variation of MSE and R with the number of hidden neurons for SCG-BP.

As shown in Figure 3, when the number of hidden layer nodes is 10, the MSE of the predicted and true values of output torque and eddy current loss in the test set reach their minimum values of 0.00162507 and 0.0654804, respectively, and the regression values R reach their maximum values of 0.998752 and 0.999313, respectively. The values of the above indicators correspond to the values circled in the four circles in Figure 3. Therefore, the

number of hidden layer nodes in the neural network model for output torque and eddy current loss is set to 10.

(4)   Number of neurons in the output layer. The number of neurons in the output layer is determined by the output results.

In this section, two neural network structures will be built with the two performance indicators, PMECC output torque, and eddy current loss, as outputs, respectively, so as to obtain the two required objective functions. Therefore, each performance indicator corresponds to a neural network structure, with a corresponding output node count of 1.

In summary, this paper will establish two single hidden layer SCG-BP neural networks with a structure of 4-10-1, which take parameters such as air gap width and permanent magnet thickness of PMECC as input variables and output torque and eddy current loss as output variables, respectively. Set the number of iterations of the neural network to 10,000, the dynamic factor to 0.9, the learning rate to 0.01, the performance function of the network to "MSE", and the training function to "trainscg".

2.2. Output of Results and Error Analysis

Figures 4 and 5 show the MSE and R obtained from the SCG-BP process for solving the PMECC output torque and eddy current loss for the test and validation sets of regression plots. The optimal values of MSE for output torque and eddy current loss are presented at epoch 112 and epoch 96, 0.0016251 and 0.06548, respectively. The corresponding points are shown in the two green circles in Figure 4a,b. The values of R for the test and validation sets of output torque are 0.99832 and 0.99875, respectively, and the values of R for the test and validation sets of eddy current loss are 0.99915 and 0.99931, respectively.

Best Validation Performance is 0.0016251 at epoch 112 Best Validation Performance is 0.06548 at epoch 96

(**a**) Output torque
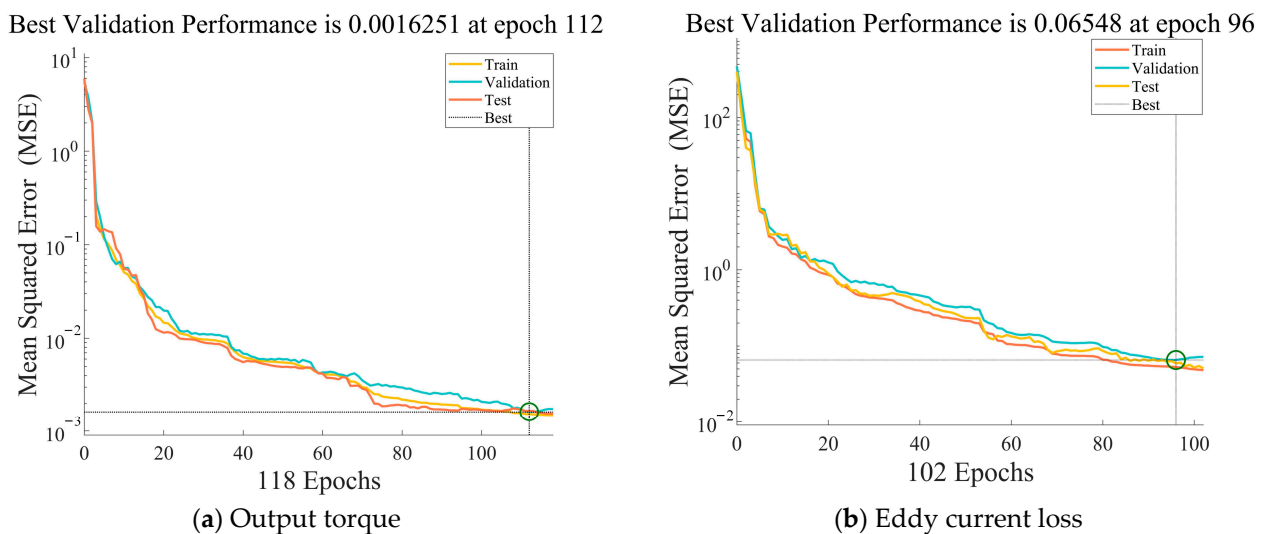
(**b**) Eddy current loss

Figure 4. MSE of SCG-BP model for output torque and eddy current loss.

From Figure 5, it is evident that the predicted values and sample values have a high correlation.

The above results indicate that the SCG-BP neural network used in this paper has good predictive performance and can accurately reflect the nonlinear relationship between the parameters of PMECC and its output torque and eddy current loss. Therefore, it can be used as an effective model for predicting the objective function of output torque and eddy current loss.

(**a**) Output torque
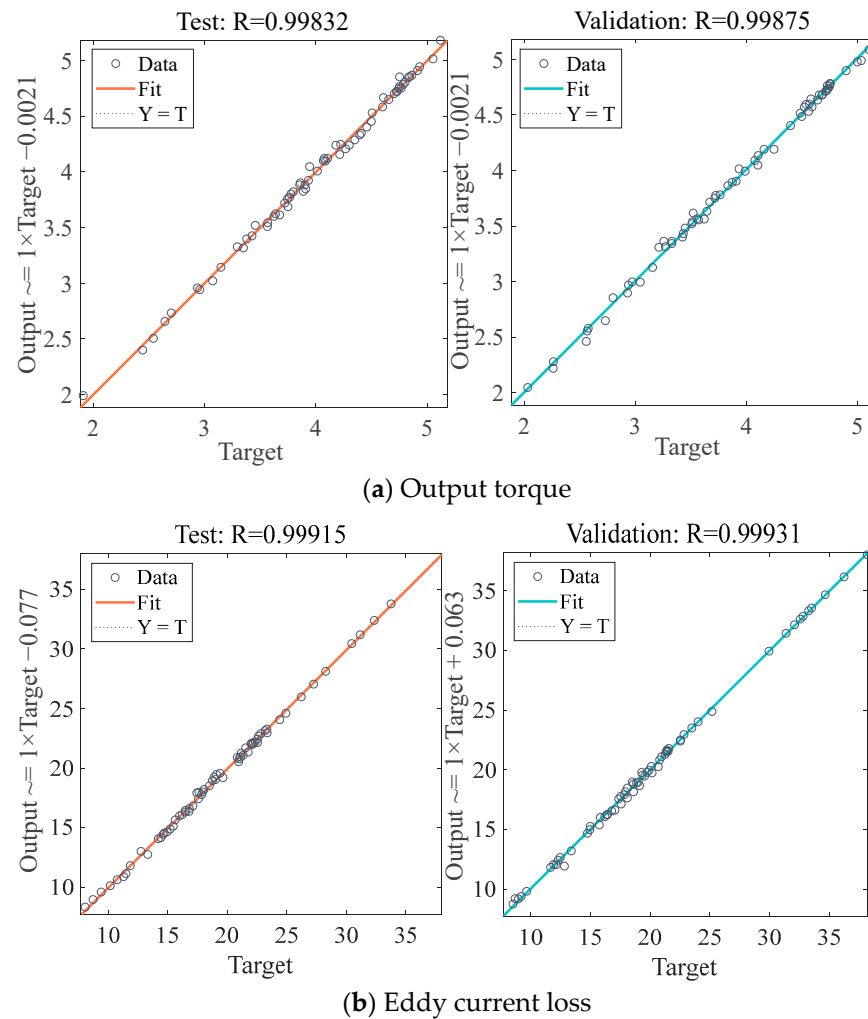
(**b**) Eddy current loss

Figure 5. SCG-BP testing and validation set regression for output torque and eddy current loss.

3. The NSGA-II Algorithm with an Improved Opposition-Based Learning Mechanism and NDX Crossover Operator

This section introduces a fast, non-dominated multi-objective optimization algorithm (NSGA-II genetic algorithm) to optimize the output torque, eddy current loss, and cost of PMECC. Compared with multi-objective particle swarm optimization (MOPSO) and multi-objective differential evolution algorithm (MODE), the NSGA-II algorithm has a strong global search ability and can provide a better global optimal solution [21]. However, the NSGA-II algorithm also has some shortcomings. It cannot guarantee the diversity of searches, and the convergence speed is slow. Therefore, we introduce an improved opposition-based learning mechanism and NDX cross operator to improve the traditional NSGA-II algorithm.

3.1. Improved Opposition-Based Learning Mechanism

Opposition-based learning (OBL) was first proposed by HR Tizhoosh et al. in 2006 [22]. It has been proven to accelerate the convergence rate of heuristic optimization algorithms. Its mathematical model is shown as follows:

Assuming $X = (x_1, x_2, \cdots, x_n)$ is a solution vector on the n-dimensional solution space, with $x_i \in [L_i, U_i]$, $\forall i \in (1, 2, \cdots, n)$, then the opposite solution of X is $X' = (x'_1, x'_2, \cdots, x'_n)$, where the vector element is:

$$x'_i = L_i + U_i - x_i \tag{2}$$

In the equation, L_i and U_i represent the lower and upper limits of the search domain, respectively. The above mathematical model is shown in Figure 6.
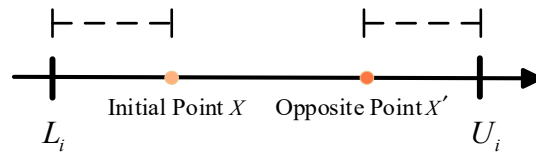
Figure 6. Generation of opposite point in opposition-based learning mechanism.

In this paper, the opposition-based learning mechanism is applied to the entire population evolution process, including the initialization, crossover, and mutation processes. This facilitates the expansion of the range of feasible solutions and enhances the diversity as well as the quality of the populations in each generation, resulting in better performance of the algorithm.

In addition, considering that the population P in the later stage of evolution has approached the optimal solution region, calculating its opposite solution for all individuals will undoubtedly greatly slow down the convergence speed of the population. Therefore, we introduce the dynamic factor ε in the opposition-based learning of the evolutionary process, which decreases with the evolution of the population. The expression ε is shown in Equation (3).

$$\varepsilon = \max\varepsilon - \frac{g}{G}(\max\varepsilon - \min\varepsilon) \tag{3}$$

In the equation, G is the maximum number of iterations for the population, g is the current number of iterations, $\max\varepsilon$ is the maximum value of the dynamic factor, $\max\varepsilon = 1$, and $\min\varepsilon$ is the minimum value of the dynamic factor.

From Equation (3), it can be seen that as the population evolution algebra increases, the value of dynamic factors gradually decreases. However, if the difference between each individual is taken into account, the more posterior the dominant relationship in the population is, the better the opposite solution is likely to perform, so that the individual should have a greater opposite learning probability. Therefore, under the original trend of ε changes, the size of $\min\varepsilon$ will also be dynamically adjusted based on the number of dominant layers in each individual. The value of $\min\varepsilon$ is:

$$\min\varepsilon = \frac{rank\ l_i}{l_T} \cdot \max\varepsilon \tag{4}$$

In the equation, $rank\ l_i$ is the number of dominant layers of the i-th individual in the N-th individual, and l_T is the total number of dominant layers of the current generation.

In this way, the opposition-based learning probability of an individual can dynamically vary with the number of dominance layers while decreasing with the number of evolutionary generations. This can effectively ensure the convergence speed of the algorithm while taking into account the differences of each individual during the evolution process.

3.2. Cross Operator Based on NDX

The crossover operator used in the real number encoding of NSGA-II is the simulated binary crossover operator, abbreviated as the SBX operator. It is defined as: for parents $x^1 x^2$, to generate children, c^1 and c^2 in the following way:

$$\begin{cases} c_i{}^1 = \left[(1+\beta)x_i{}^1 + (1-\beta)x_i{}^2\right]/2 \\ c_i{}^2 = \left[(1-\beta)x_i{}^1 + (1+\beta)x_i{}^2\right]/2 \end{cases}, 1 \leq i \leq n \tag{5}$$

In Equation (5), βa random variable is dynamically generated by the distribution factor η. Therefore, its search range is limited, making it prone to problems such as local optimums and unstable evolutionary processes [23] due to the shortcomings of the SBX operator. This paper introduces the normal distribution into the crossover operation SBX,

that is, the space search capability is enhanced by using $1.481|N(0,1)|$a parameter instead of a parameter β to expand the search space, and $N(0,1)$ is a normal distribution random variable [24]. Equation (5) can be expressed as follows:

$$c_{1/2,i} = (x_{1,i} + x_{2,i})/2 \pm 1.481(x_{1,i} - x_{2,i})/2|N(0,1)| \tag{6}$$

3.3. ONDX-NSGA-II Algorithm

3.3.1. Steps of ONDX-NSGA-II Algorithm

Based on the above analysis, this paper improves the traditional NSGA-II algorithm in two aspects. On the one hand, it accelerates the convergence speed of the algorithm by introducing an improved opposition-based learning mechanism so that the algorithm can find the optimal solution better, enhance the global search ability of the algorithm, and improve the learning rate. On the other hand, by introducing the NDX crossover operator, the algorithm can more easily jump out of the local optimum and improve the quality of the Pareto frontier solution.

The NSGA-II algorithm incorporating the improved opposition-based learning mechanism and the NDX operator proceeds is shown in Figure 7.
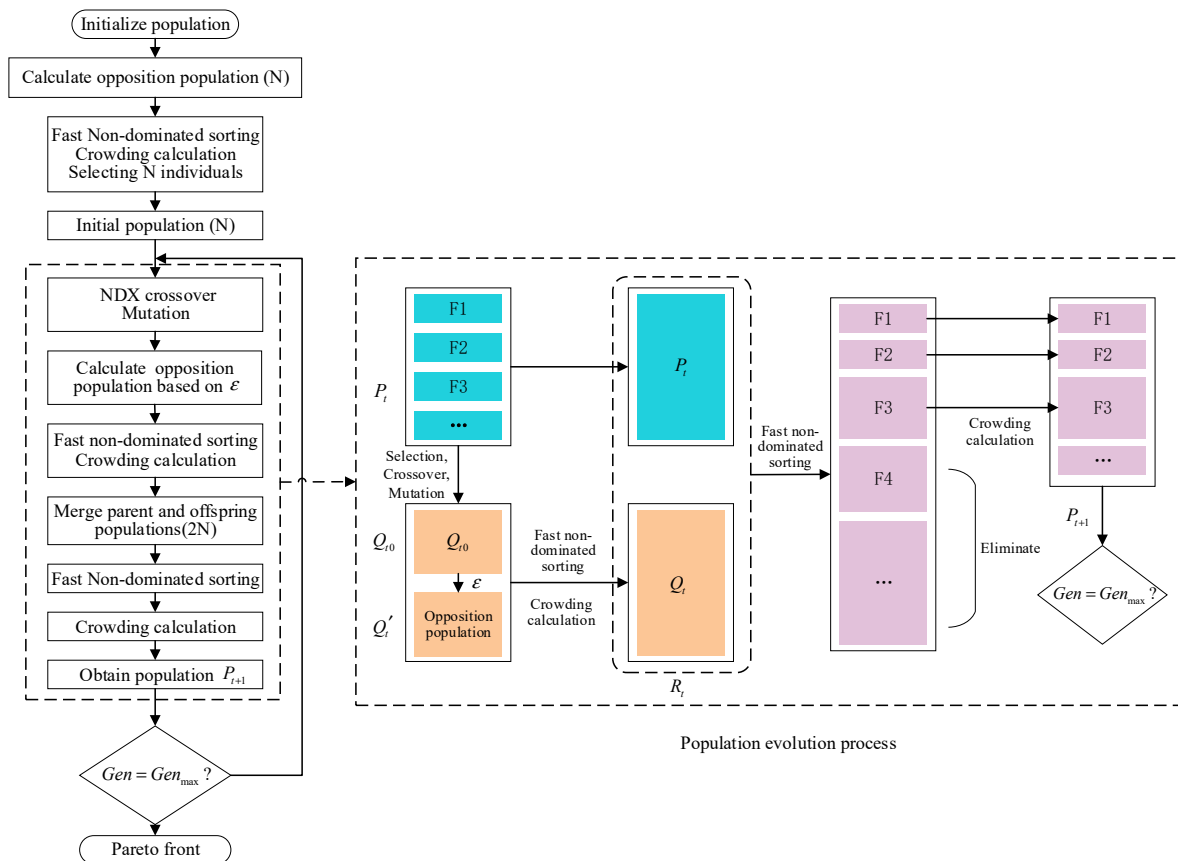
Figure 7. Flowchart of ONDX-NSGA-II optimization algorithm.

3.3.2. Establishment of Objective Function

Before the structural parameters of the PMECC can be optimally designed with multiple objectives, it is necessary to construct comprehensive evaluation indicators. For PMECC, output torque and copper disk eddy current loss are the most important evaluation indicators. Among all losses, copper disk eddy current loss accounts for the main proportion of PMECC energy conversion and has the most important impact on the performance of PMECC. Therefore, we chose copper disk eddy current loss as one of the optimization objectives without calculating other loss terms for PMECC, such as PM loss and iron loss [25]. In addition, the cost indicators of PMECC cannot be ignored. The cost of PMECC is directly

related to its volume; therefore, we use volume calculation instead in the cost calculation process. Meanwhile, considering the difference between the price of the permanent magnet material and the price of the copper conductor, the objective function is calculated by multiplying the volume of the permanent magnet by a factor of 10, so that the cost objective function [26] is expressed as:

$$
\begin{aligned}
C &= 10V(\mathrm{NdFeB}) + V(\mathrm{Cu}) \\
&= 10W_{pm}H_{pm}D_{pm}N + \pi(R_{cop} - r_{cop})^2 h_{cop}
\end{aligned}
\tag{7}
$$

In the equation, W_{pm} is the radial length of the permanent magnet, H_{pm} is the height of the permanent magnet, D_{pm} is the thickness of the permanent magnet, N is the number of permanent magnets, R_{cop} is the outer diameter of the copper disk, r_{cop} is the inner diameter of the copper disk, and h_{cop} is the thickness of the copper disk.

Therefore, we use the output torque, eddy current loss and the cost of PMECC as optimization indicators. The objective functions of output torque and eddy current loss are fitted by the SCG-BP neural network, represented by T and P_{loss}, respectively. And the volume expression of PMECC is shown in Equation (7).

Based on the above analysis, a multi-objective optimization mathematical model for PMECC can be established, as shown in Equation (8).

$$
\begin{cases}
\max T = f_1(X) \\
\min P_{loss} = f_2(X) \\
\min C = f_3(X)
\end{cases}
\tag{8}
$$

In the equation, $X = (x_1, x_2, x_3, x_4)$, x_1 represents the width of the air gap in mm, x_2 represents the thickness of the copper disk in mm, x_3 represents the thickness of the permanent magnet in mm, and x_4 represents the relative slip in rpm.

In order to make the optimization design more reasonable, a series of constraint conditions are defined, taking into account factors such as eddy current density limitations and volume size limitations. The constraints of the mathematical model are shown in Equation (9).

$$
\begin{cases}
2 \leq x_1 \leq 10 \\
4 \leq x_2 \leq 12 \\
10 \leq x_3 \leq 52 \\
25 \leq x_4 \leq 75
\end{cases}
\tag{9}
$$

The specific structural parameters of PMECC are shown in Table 1.

Table 1. Standard model structural parameters.

Model Parameter	Value	Model Parameter	Value
Material of copper	BrassH62	Permanent magnet material	NdFeB
Inner radius of copper disk/mm	190	Relative slip/rpm	45
Outer radius of copper disk/mm	370	Thickness of copper disk/mm	8
Number of permanent magnets	18	Airgap gap width/mm	4
Radial length of permanent magnet/mm	130	Thickness of permanent magnet/mm	25
Height of Permanent magnet/mm	68	Inner radius of back iron/mm	190

3.4. Optimal Results

The parameter settings of the ONDX-NSGA-II algorithm used are as follows: The population size is set at 300. The mutation probability of the mutation operator is set to 0.2, and the maximum number of iterations is set to 100. The optimized Pareto frontier is shown in Figures 8 and 9.
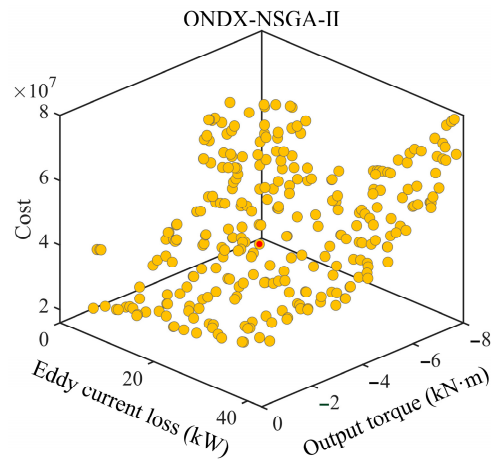
Figure 8. Approximately 3-D Pareto frontier solution set of ONDX-NSGA-II.
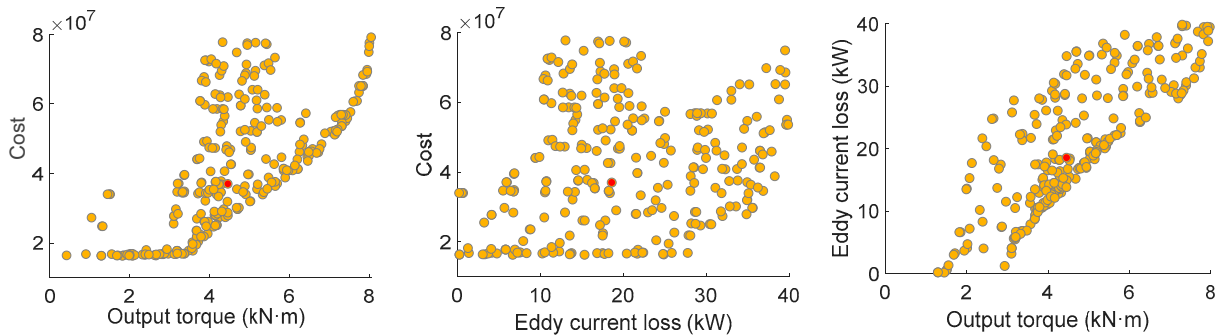
Figure 9. Approximately 2-D Pareto frontier solution set of ONDX-NSGA-II.

After optimizing the four structural parameters of the PMECC, the optimal point on the Pareto frontier solution set is selected after taking into account maximum output torque with minimum eddy current loss and cost. This point is the optimal solution obtained from this optimization. The red point marked in Figures 8 and 9 is the optimal solution.

Due to the fact that multi-objective optimization is a highly stochastic process, the parameter changes of each individual will vary in different iterations due to the randomness of the algorithm. Additionally, the individual may also be directly eliminated or replaced during the evolution process. Therefore, this paper does not describe the parameter evolution process for each individual.

Table 2 shows the comparison of performance indicators before and after PMECC optimization. The structural parameters corresponding to this point are: air gap width is 2 mm; copper disk thickness is 6.84 mm; permanent magnet thickness is 22.84 mm; and relative slip is 40.58 rpm.

Table 2. Comparison of performance indicators before and after optimization.

	Before Optimization	After Optimization	Variation (%)
Output torque/kN·m	4.1015	4.4517	8.54
Torque density/N·m/cm^3	0.25616	0.29095	13.58
Eddy current loss/kW	19.3027	18.586	3.71
Cost	40,593,888	37,045,484.93	8.74

When researching and designing PMECC, the torque density within the volume is also a key performance parameter, which directly affects the volume cost and efficiency of the system. When optimizing, our goal is to maximize the output torque and minimize the cost of approximate substitution with volume indicators. Therefore, the optimal solution we ultimately obtain can also represent the solution with the highest torque density in

PMECC. We have also provided comparative results for torque density in the optimization results. The torque density within a volume refers to the distribution of torque within a given volume, and its calculation formula is as follows:

$$\tau = \frac{T}{V}$$

where τ is the torque density in $N \cdot m/cm^3$, T is the output torque, and V is the volume of space occupied by PMECC.

The volume of PMECC is expressed as:

$$V = V_{iron} + V_{PM} + V_{copper}$$
$$= 2 \times (R_{oi}{}^2 - R_{ii}{}^2) \times \pi h_i + 18 R_{PM} T_{PM} H_{PM} + (R_{oc}{}^2 - R_{io}{}^2) \times \pi h_c$$

According to Table 2, compared with the coupler before optimization, the ONDX-NSGA-II algorithm optimized the results to achieve the goal of lower eddy current loss and cost in the case of larger output torque and torque density. This indicates that optimizing the structural parameters of PMECC is very meaningful.

In addition, we also calculated the efficiency of PMECC before and after optimization to comprehensively measure its performance improvement. The input power of PMECC is the output power of the prime mover, mainly divided into two parts: eddy current loss and output power [27]. The efficiency of PMECC can be calculated as follows:

$$\eta = \frac{P_{out}}{P_{out} + P_{loss} + P_{iron}} \times 100\%$$

The output power P_{out} is expressed as:

$$P_{out} = \frac{T * n}{9550}$$

Among them T is the output torque, which n represents the speed of the copper disk.

P_{loss} can be directly obtained from the previous data, and according to the subsequent calculations in Reference [27], it is known that the eddy current loss is much greater than the loss of iron; therefore, the loss of iron can be ignored.

Therefore, it can be calculated that the efficiency of the PMECC before and after optimization is $\eta_{before} = 97.00\%$, $\eta_{after} = 97.34\%$ respectively. The efficiency has increased by 0.34%, indicating that after optimization, the PMECC has improved energy efficiency and reduced energy consumption, proving the effectiveness and feasibility of the optimization method proposed in this paper.

3.5. Comparison of Optimization Results

In order to verify the superiority of the ONDX-NSGA-II algorithm, it is compared with the PESA-II algorithm and the traditional NSGA-II algorithm. The Pareto frontier solutions obtained by Pareto envelope-based selection algorithm-II (PESA-II) and the traditional NSGA-II algorithm are shown in Figures 10 and 11. Through comparison, it can be seen that, due to the wider search space of the ONDX-NSGA-II algorithm, the Pareto optimal solution has better distribution and a high quality of solution.
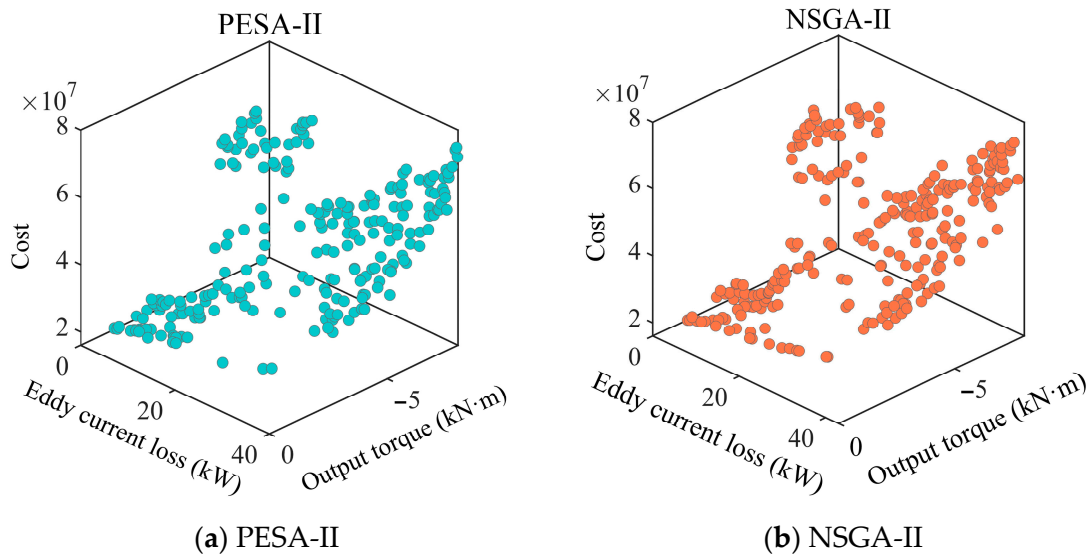
(**a**) PESA-II

(**b**) NSGA-II

Figure 10. Approximately 3-D Pareto frontier solution set of PESA-II and NSGA-II.
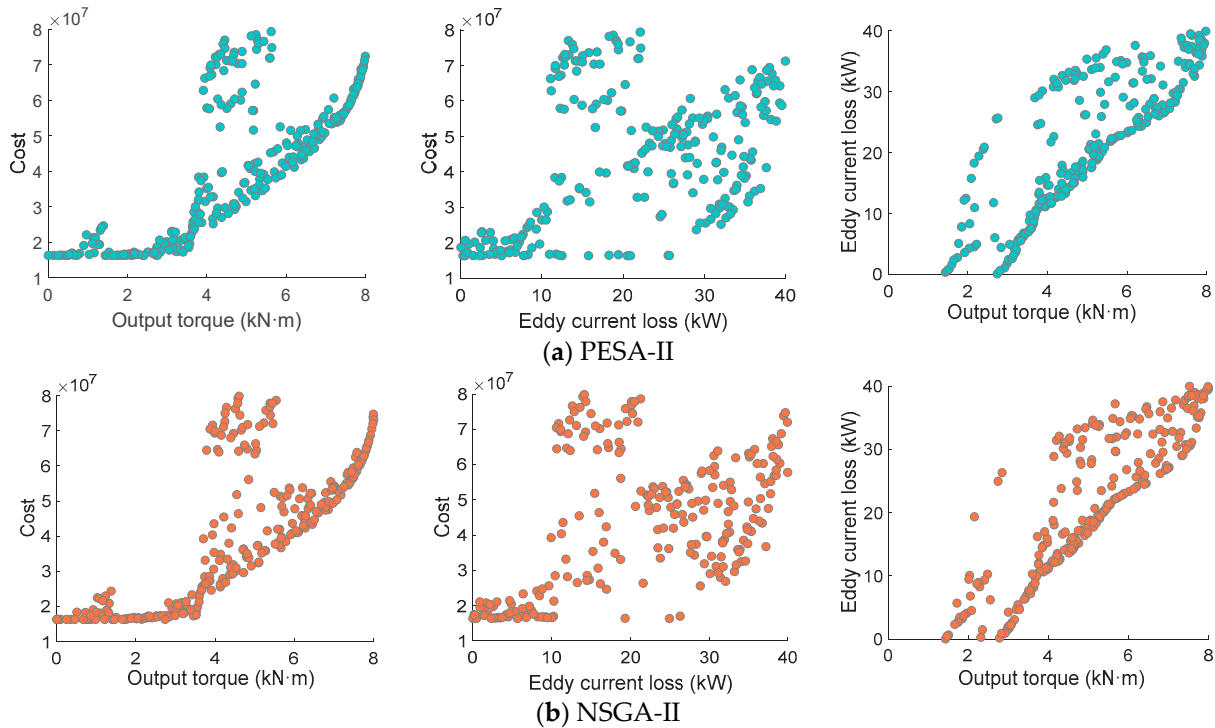
(**a**) PESA-II

(**b**) NSGA-II

Figure 11. Approximately 2-D Pareto frontier solution set of PESA-II and NSGA-II.

After comparing the pareto frontier solutions of the three algorithms, the validity and reliability of the proposed algorithm are verified in quantitative terms. The Inverted Generational Distance (IGD) [28] and Hypervolume (HV) indicators are used as indicators to evaluate the performance of the algorithm.

IGD is a comprehensive performance evaluation indicator that takes into account the convergence and diversity of the approximate solution set. The smaller the value of IGD, the better the convergence of the Pareto frontier obtained by the algorithm and the more uniform the distribution. The HV indicator is a hypervolume metric that represents the volume of the hypercube formed by individuals and reference points in the target space in the solution set obtained by the algorithm. It is mainly used to measure the diversity of the solution set. The larger the HV value, the better the diversity of the Pareto frontier solution set obtained.

Figure 12 shows the IGD and HV convergence curves of the ONDX-NSGA-II algorithm compared to the other two algorithms. It can be clearly seen that as the number of evolutions increases, the IGD convergence curve value of the ONDX-NSGA-II algorithm is smaller, while the HV value is the largest during the evolution process, indicating that the algorithm has better convergence and diversity.

(**a**) IGD

(**b**) HV
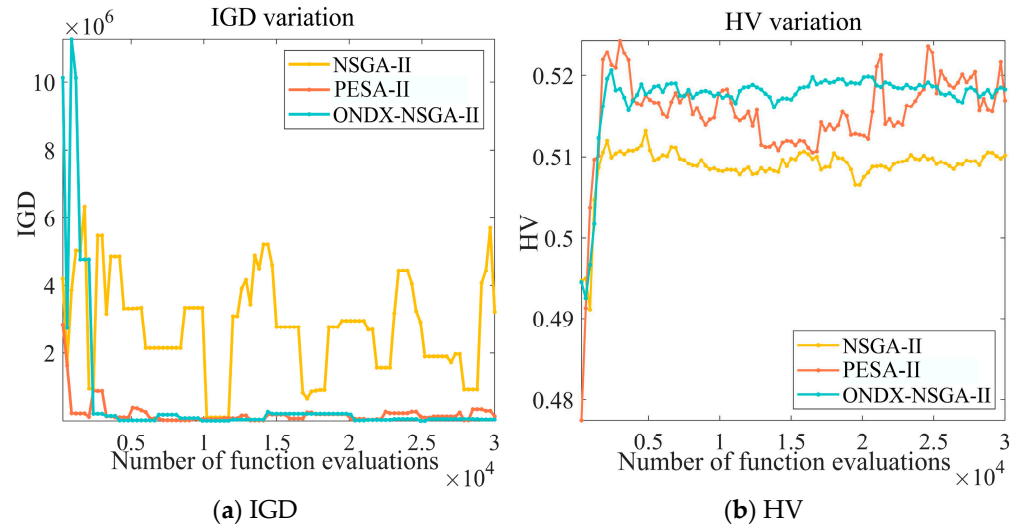
Figure 12. IGD and HV convergence curves of three algorithms.

4. Simulation Verification

4.1. ANSYS Verification

This section verifies and analyzes the results of multi-objective optimization. Using ANSYS software to conduct finite element modeling of PMECC, the established model is shown in Figure 13.
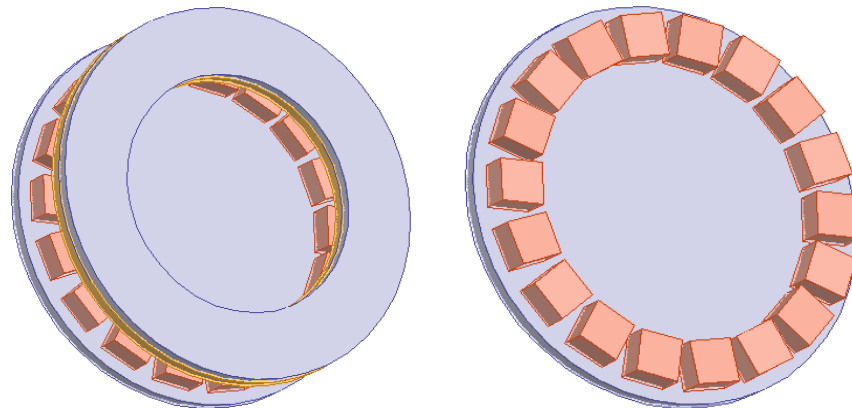
Figure 13. Finite element model of PMECC.

After establishing the ANSYS model of PMECC, the various structural parameters after optimization are imported into the model, and the output torque and eddy current loss obtained are shown in Figure 14.

(**a**) Output torque
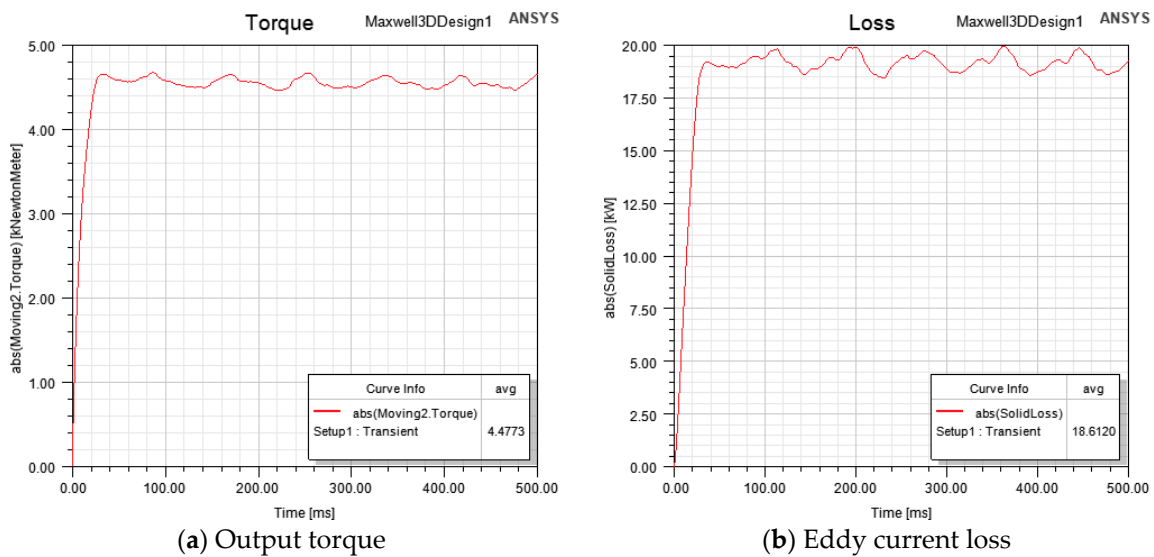
(**b**) Eddy current loss

Figure 14. Simulation value of PMECC after optimization.

Through simulation comparison, it can be seen that the output torque and eddy current loss of PMECC have been significantly improved after optimization.

Compare the data obtained from the optimization in Section 3.4 with the results obtained from establishing the finite element model in this part, and the results are shown in Table 3. The data shows that the error between the output torque and eddy current loss calculated using the ONDX-NSGA-II algorithm and the calculated values of the finite element model is less than 1%, and the two data are almost identical. The reasons for the errors are as follows:

- There are differences between the established model and the actual model.
- There are power losses during the simulation verification.

Table 3. Comparison of ONDX-NSGA-II Optimization Data and Finite Element Modelling.

	ONDX-NSGA-II	Finite Element	Error (%)
Output torque/kN·m	4.4517	4.4773	0.56
Eddy current loss/kW	18.586	18.6120	0.14

In summary, based on the error results, it can be concluded that using the ONDX-NSGA-II algorithm to optimize PMECC results is reliable.

Figure 15 is the distribution diagram of the eddy current density generated on the PMECC conductor disk before and after optimization. The induced current in the copper disk, also known as eddy current, plays a very important role in the operation of PMECC. Firstly, the conductor rotor and the permanent magnet rotor are connected through an air gap coupling. By adjusting the air gap, the force between the permanent magnet magnetic field and the magnetic field generated by the induced current is changed, and the output torque and speed are controlled in real-time. Secondly, one of the main performance parameters of PMECC, eddy current loss, is generated due to the presence of eddy currents. Therefore, the analysis of eddy currents generated by PMECC conductors is very important.

From Figure 15, it can be seen that the optimized PMECC copper disk has significantly higher eddy current density, and the drag force between magnetic fields increases, thereby improving the output torque. At the same time, the distribution of eddy currents is more uniform, and the density of stray eddy currents is reduced, thereby reducing eddy current losses.

(**a**) Before optimization

(**b**) After optimization
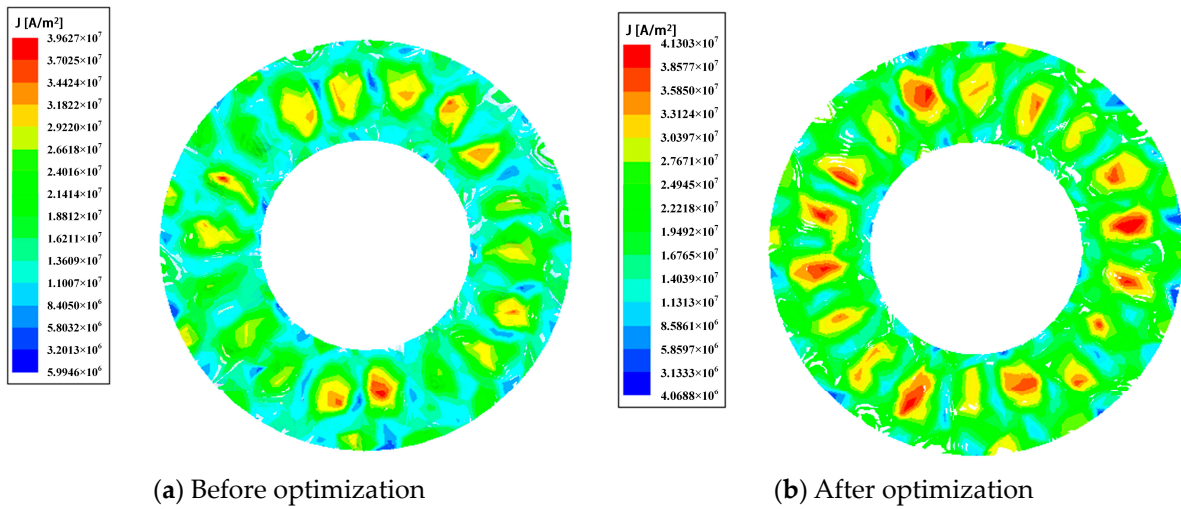
Figure 15. Eddy current density distribution of PMECC before and after optimization.

Figure 16 is the vector diagram of the distribution of magnetic field intensity before and after optimization. As the structural parameters of PMECC have changed after optimization, the performance of PMECC has been improved, the eddy current is more concentrated, and the eddy current density has increased significantly, which makes the magnetic field intensity and magnetic flux density of PMECC significantly improved, which is more conducive to generating greater output torque.

(**a**) Before optimization

(**b**) After optimization
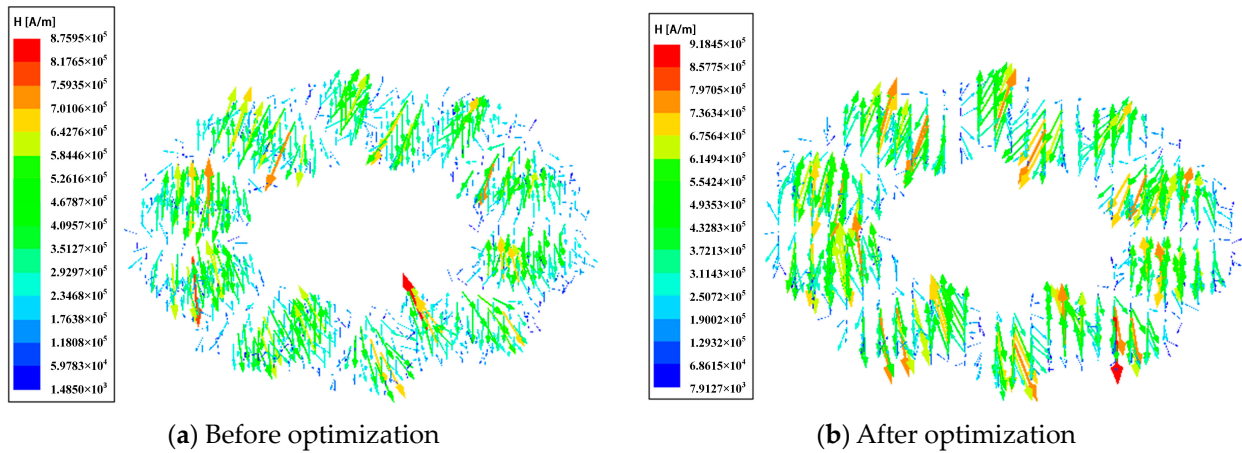
Figure 16. Vector plot of PMECC magnetic field intensity before and after optimization.

The output torque of the optimized PMECC is 4.4773 kN·m, and the eddy current loss is 18.6120 kW by using ANSYS. It can be seen that the optimized PMECC had increased output torque by 0.3758 kN·m and reduced eddy current loss by 0.6907 kW compared to the original machine. This further demonstrates the practicality and rationality of the optimization algorithm proposed in this paper for the multi-objective optimization problem of PMECC.

4.2. Experimental Testing Results

To confirm the validity of the analytical model, the experiments are carried out on the experimental simulation platform shown in Figure 17.
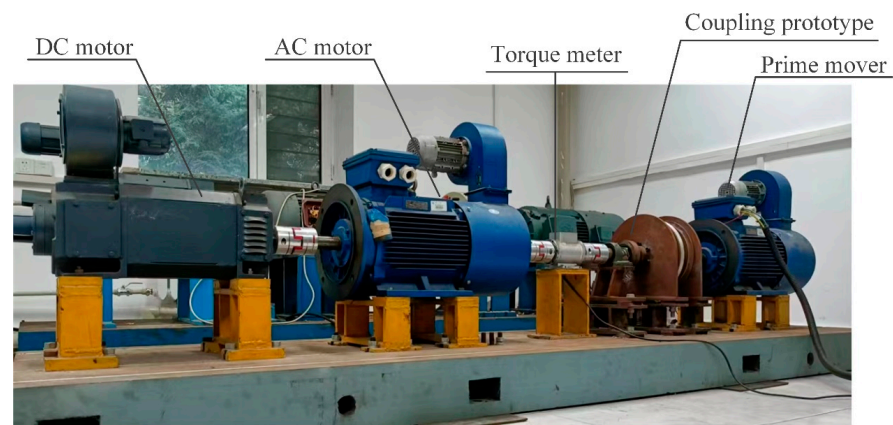
Figure 17. Permanent magnet eddy current coupler experimental platform.

Based on the fixed parameters of PMECC shown in Table 1, the structural parameters can be obtained. Considering the limitations of processing conditions (the machining size of all parts is accurate to 0.02 mm), the PMECC prototype is designed, and the experimental platform is built. The overall structure of the experimental platform is shown in Figure 17. The main equipment includes a DC motor, an AC motor, a torque meter, a PMECC, and a prime mover. Among them, the DC motor and the DC governor simulate the load, and the torque meter is used to measure the torque and speed of the output of the PMECC. The PMECC is installed between the prime mover and the torque meter. The rated power of the prime mover is 15 kW, and the rated speed is 1500 rpm. Adjust the PMECC air gap to 4 mm, and when the slip reaches 45 rpm, use a torque meter to record the output torques of the prime mover and PMECC at corresponding speeds of 4.0893 kN·m and 4.0872 kN·m, respectively. Then, calculate the corresponding transmission efficiency, and the test data is $\eta_{\exp eriment} = 96.95\%$, which shows the loss of the mechanical parts of the PMECC. Meanwhile, by comparing the transmission efficiency of this section with the values obtained from finite element simulation, it can be concluded that the transmission efficiency of the experimental platform is slightly lower than the efficiency obtained from finite element calculation; however, the difference between the two is small, which verifies that this paper uses the finite element method to analyze the correctness and reasonableness of the PMECC.

Subsequently, in order to further verify the effectiveness of finite element simulation, we measured the output torque of PMECC under different slip through the experimental simulation platform and compared it with the finite element simulation results.

At the same time, the three-dimensional finite element model of PMECC before optimization is established according to Table 1.

A numerical simulation of output torque under different slip is performed on the established 3D finite element model, and the results are compared with the experimental results obtained from the experimental platform, as shown in Figure 18. The slip corresponding to the points marked in Figure 18 is the slip selected for the comparative experiment.

According to the above comparison results, it can be seen that the ANSYS simulation value of the model before optimization has good consistency with the simulation results of PMECC output torque under different slips obtained from the experimental platform. It further confirms the accuracy and reliability of the simulation model and the validity of the simulation method we have adopted.
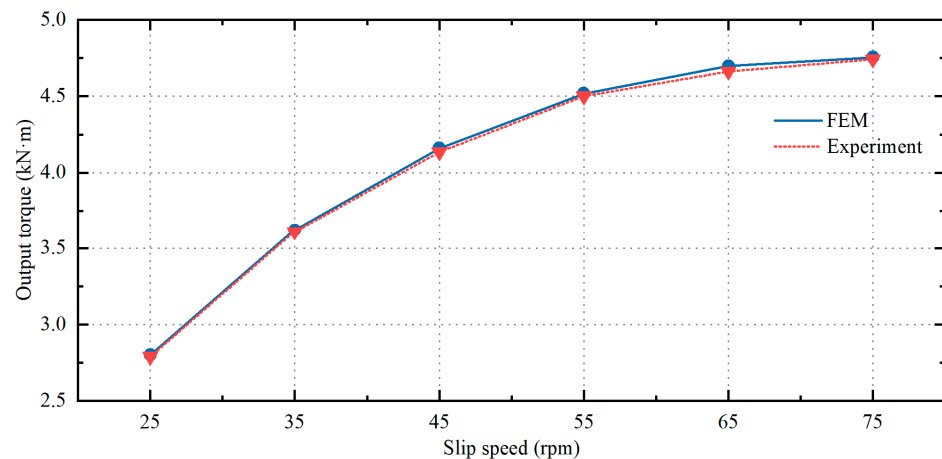
Figure 18. Experimental results of output torque under different slips.

5. Conclusions

This paper conducted research on multi-objective optimization of PMECC performance indicators and proposed an ONDX-NSGA-II multi-objective optimization method based on SCG-BP neural network modeling. Firstly, the SCG-BP neural network was used to model PMECC, and a nonlinear regression model of PMECC output torque and eddy current loss was obtained. Secondly, the improved opposition-based learning mechanism and NDX crossover operator were introduced into the NSGA-II algorithm, and the ONDX-NSGA-II multi-objective optimization algorithm was proposed. During the optimization process, the structural parameters of PMECC were used as design variables, with output torque, eddy current loss, and cost as optimization objectives. The overall performance of the optimized PMECC had greatly improved compared to before optimization. Compared with the traditional NSGA-II algorithm and PESA-II algorithm, the proposed multi-objective optimization algorithm has a wider search space, a better distribution of the Pareto optimal solution, and can effectively solve the problems of slow convergence, easy local optimality, and unstable evolutionary processes.

In order to further verify the effectiveness and correctness of the algorithm, this paper used the finite element simulation software ANSYS to carry out simulation verification of the optimized results. A three-dimensional finite element model of PMECC was established using the optimized structural parameters. The final optimized output torque and eddy current losses were found to be less than 1% compared to the simulated data. In addition, the distribution of flux density and eddy current density of the PMECC before and after the improvement were compared. It was found that the PMECC with the optimized structure parameters can achieve a higher output torque with relatively low eddy current loss and cost. Through the comparison and validation of results between finite element simulation experiments and experimental simulation platforms, the effectiveness and reliability of the proposed PMECC multi-objective optimization method are further confirmed, which is of great significance for the future design and structural optimization of PMECC.

Author Contributions: Conceptualization, D.W. and B.N.; methodology, D.W., B.N. and P.P.; software, B.N. and P.P.; validation, B.N. and P.P.; formal analysis, D.W. and B.N.; investigation, D.W., B.N., P.P. and G.S.; resources, D.W. and G.S.; data curation, B.N., G.S. and P.P.; writing—original draft preparation, D.W. and B.N.; writing—review and editing, D.W., B.N., P.P. and G.S.; visualization, B.N. and P.P.; supervision, D.W.; project administration, D.W. and G.S.; funding acquisition, D.W. and G.S. All authors have read and agreed to the published version of the manuscript.

Data Availability Statement: The data presented in this study are available on request from the corresponding author.

Conflicts of Interest: The authors declare no conflict of interest. The funders had no role in the design of this study, in the collection, analysis, or interpretation of data, in the writing of the manuscript, or in the decision to publish the results.

References

1. Choi, J.Y.; Shin, H.J.; Jang, S.M. Torque analysis and measurements of cylindrical air-gap synchronous permanent magnet couplings based on analytical magnetic field calculations. *IEEE Trans. Magn.* **2013**, *49*, 3921–3924. [CrossRef]
2. Wang, J.; Zhu, J.S. A simple method for performance prediction of permanent magnet eddy current couplings using a new magnetic equivalent circuit model. *IEEE Trans. Ind. Electron.* **2018**, *65*, 2487–2495. [CrossRef]
3. Wang, D.M.; Meng, Q.R.; Hou, Y.F. Transient temperature field of magneto-rheological fluid in transmission device. *Trans. Chin. Soc. Agric. Mach.* **2013**, *44*, 287–292.
4. Tsai, M.C.; Chiou, K.Y.; Wang, S.H. Characteristics measurement of electric motors by contactless eddy current magnetic coupler. *IEEE Trans. Magn.* **2014**, *50*, 1–4. [CrossRef]
5. Mo, L.; Zhu, X.; Zhang, T. Temperature rise calculation of a flux-switching permanent-magnet double-rotor machine using electromagnetic-thermal coupling analysis. *IEEE Trans. Magn.* **2018**, *54*, 8201004. [CrossRef]
6. Wang, J. A generic 3-d analytical model of permanent magnet eddy current coupling using a magnetic vector potential formulation. *IEEE Trans. Ind. Electron.* **2021**, *99*, 663–672. [CrossRef]
7. Jang, G.H.; Kim, J.M.; Shin, H.J. Optimal design and torque analysis considering eddy-current reduction of axial-flux permanent magnet couplings with Halbach array based on 3D-FEM. In Proceedings of the 2016 IEEE Conference on Electromagnetic Field Computation (CEFC), Miami, FL, USA, 13–16 November 2016; p. 1.
8. Li, Z.; Wang, D.Z.; Zheng, D. Analytical modeling and analysis of magnetic eld and torque for novel axial flux eddy current couplers with PM excitation. *AIP Adv.* **2017**, *7*, 105303. [CrossRef]
9. Xu, L.; Liu, G.H.; Zhao, W.X. Analysis of new modular linear flux reversal permanent magnet motors. *IEEE Trans. Magn.* **2015**, *51*, 1–4.
10. Tian, C.H.; Zhong, Y.H.; Wei, L.L. A coupled method for evaluating eddy current loss of NdFeB permanent magnets in a saturated core fault current limiter. *IEEE Trans. Magn.* **2017**, *53*, 6300504. [CrossRef]
11. Aberoomand, J.; Mirsalim, M.; Fesharakifard, R. Design optimization of double-sided permanent-magnet axial eddy-current couplers for use in dynamic applications. *IEEE Trans. Energy Convers.* **2019**, *34*, 909–920. [CrossRef]
12. Wang, J.; Lin, H.Y.; Fang, S.H. A general analytical model of permanent magnet eddy current couplings. *IEEE Trans. Magn.* **2014**, *50*, 1–9. [CrossRef]
13. Amged, E. Design optimization of PM couplings using hybrid particle swarm optimization-simplex method (PSO-SM) algorithm. *Electr. Power Syst. Res.* **2014**, *116*, 29–35.
14. Wang, A.; Wang, J.B.; Wu, B. Structural optimization of the permanent magnet drive based on artificial neural network and particle swarm optimization. In Proceedings of the IEEE Conference of the Third Intelligent Human-Machine Systems and Cybernetics, Hangzhou, China, 26–27 August 2011; pp. 70–75.
15. Shi, S.N.; Wang, D.Z.; Shi, T.Y. Multi-objective parameter optimization design of permanent magnet drive. *Control Eng. China* **2014**, *21*, 369–373.
16. Li, Z.; Wang, D.Z.; Shi, T.Y. Fuzzy optimal design of axial permanent magnet coupling based on lmproved cuckoo search algorithm. *Trans. Chin. Soc. Agric. Mach.* **2015**, *46*, 378–384.
17. Shangguan, X.F.; Yang, H.Y.; Jia, X.L. Parameter analysis and multi-objective optimization design of disc permanent magnet eddy current coupler. *J. Magn. Mater. Devices* **2022**, *53*, 67–72.
18. Wang, A.; Wang, J.B.; Shi, C.L. Study on nonlinear regression modelling methods of the permanent magnet drive. In Proceedings of the 2011 International Conference on Electronics and Optoelectronics, Dalian, China, 29–31 July 2011; pp. 87–90.
19. Liu, J.G.; Huang, J.; Sun, R. Data fusion for multi-source sensors using GA-PSO-BP neural network. *IEEE Trans. Intell. Transp. Syst.* **2021**, *22*, 6583–6598. [CrossRef]
20. Zhang, S.Z.; Chen, T.Y.; Minav, T. Position Soft-Sensing of Direct-Driven Hydraulic System Based on Back Propagation Neural Network. *Actuators* **2021**, *10*, 332. [CrossRef]
21. Mohammed, M.S.; Vural, R.A. NSGA-II+FEM based loss optimization of three phase transformer. *IEEE Trans. Ind. Electron.* **2019**, *66*, 7417–7425. [CrossRef]
22. Rahnamayan, S.; Tizhoosh, H.R.; Salama, M.M.A. Opposition-based differential evolutional algorithms. In Proceedings of the 2006 IEEE International Conference on Evolutionary Computation, Vancouver, BC, Canada, 16–21 July 2006; pp. 2010–2017.
23. Herrera, F.; Lozano, M.; Sánchez, A.M. A taxonomy for the crossover operator for real-coded genetic algorithms: An experimental study. *Int. J. Intell. Syst.* **2003**, *18*, 309–338. [CrossRef]
24. Zhang, M.; Luo, W.J.; Wang, X.F. A normal distribution crossover for ε-MOEA. *J. Softw.* **2009**, *20*, 305–314. [CrossRef]
25. Wang, J.X.; Wang, D.Z.; Wang, S.H. A Review of Recent Developments in Permanent Magnet Eddy Current Couplers Technology. *Actuators* **2023**, *12*, 277. [CrossRef]
26. Yang, C.J.; Guan, C.S. Multi-objective optimization design of axial permanent magnet couplings with adjustable speed system. *Mach. Des. Res.* **2011**, *27*, 37–41.

27. Kong, D.S.; Wang, D.Z.; Li, W.H. Analysis of a novel flux adjustable axial flux permanent magnet eddy current coupler. *IET Electr. Power Appl.* **2023**, *17*, 181–194.

28. Ali, S.; Arcaini, P.; Yue, T. Do quality indicators prefer particular multi-objective search algorithms in search-based software engineering. In Proceedings of the International Symposium on Search Based Software Engineering, Lille, France, 10–14 July 2020; pp. 25–41.